ACS APPLIED MATERIALS & INTERFACES

www.acsami.org

Research Article

Photo-Driven Delivery of ^{125}I-Labeled Nanomicelles for Nucleus-Targeted Internal Conversion Electron-Based Cancer Therapy

Yuanyuan Qin,[§] Mengling Shen,[§] Xinpei Liu, Jingyu Gu, Minqian Zhu, and Xuan Yi*

Cite This: https://doi.org/10.1021/acsami.1c13249

Read Online

ACCESS | Metrics & More | Article Recommendations | Supporting Information

ABSTRACT: As a kind of high linear energy transfer (LET) radiation, internal conversion electrons are emitted from some radionuclides, such as ^{125}I, triggering severe DNA damage to tumor cells when transported into the nucleus. Herein, we develop a curcumin-loaded nanomicelle composed of a photosensitizer chlorin e6 (Ce6) and amphiphilic poly(ethylene glycol) (poly(maleic anhydride-*alt*-1-octadecene)-poly(ethylene glycol) (C_{18}-PMH-PEG)) to deliver ^{125}I into the nucleus under 660 nm laser irradiation, leading to the optimized imaging-guided internal conversion electron therapy of cancer. Ce6-containing nanomicelles (Ce6-C_{18}-PEG) self-assemble with nucleus-targeted curcumin (Cur), obtaining Ce6-C_{18}-PEG/Cur nanoparticles. After labeling Cur with ^{125}I, Ce6-C_{18}-PEG/Cur enables single-photon emission computed tomography and fluorescence imaging of the tumor, serving as a guide for follow-up laser irradiation. Notably, the 660 nm laser-triggered photodynamic reaction of Ce6 optimizes the delivery of Ce6-C_{18}-PEG/^{125}I-Cur at various stages, including tumor accumulation, cellular uptake, and lysosome escape, causing plenty of ^{125}I-Cur to enter the nucleus. By this strategy, Ce6-C_{18}-PEG/^{125}I-Cur showed optimal antitumor efficacy and high biosafety in mice treated with local 660 nm laser irradiation using efficient energy deposition of internally converted electrons over short distances. Therefore, our work provides a novel strategy to optimize ^{125}I delivery for tumor treatment.

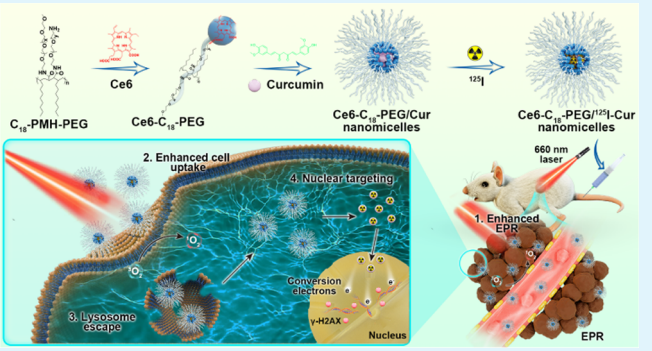

KEYWORDS: *high LET, nucleus targeting, photodynamic therapy, nanomicelle, cancer theranostics*

INTRODUCTION

Radiotherapy consisting of external beam radiotherapy (EBRT) and radionuclide therapy (RNT) has been adopted to treat 50% of cancer patients, prolong their survival time, and improve their quality of life.[1−4] Ionizing radiation used in radiotherapy is classified as high linear energy transfer (LET) radiation (>10 keV/m) and low LET radiation (<10 keV/m), according to the physical amount of the radiation force acting on the substance.[5] Generally, the relative biological effectiveness of radiation positively correlates with its LET (<100 keV/μm). Meanwhile, the oxygen enhancement ratio of ionizing radiation gradually decreases with the LET increase. Given these characteristics, high LET radiation, such as proton-heavy ion beam, has shown an apparent advantage in EBRT for cancer treatment, especially against hypoxic tumor cells.[6−8] High LET radiation, including α rays, Auger electrons, and internal conversion electrons, can be emitted from radionuclides and applied in the RNT of cancer.[9,10] Owing to their limited action range of high LET electrons, the ideal therapeutic effect of RNT can only be obtained when they are delivered near the nucleus.[11] However, in practice, free radionuclides or radionuclide-labeled nucleus-entering micromolecules, including nucleus-targeting polypeptides, DNA-targeting drugs, and strong colorants, possess limited blood circulation time and nonspecific distribution *in vivo*.[12−17]

In recent years, nanomicelles have attracted a great deal of attention as promising antitumor drug vehicles.[18−20] These highly biocompatible nanocarriers can be loaded with diverse diagnostic/therapeutic agents for imaging-guided precise cancer treatment.[21−23] However, during the nucleus-targeted delivery of chemotherapeutics or radioisotopes, these nanoparticles encounter various biological barriers such as mononuclear phagocyte system, tumor vasculature, tumor cell membrane, endosomes, and nuclear envelope.[24−26] Thus, multiple strategies, including surface modification of nanoparticles and internal/external environmental stimulus, have been explored to enhance drug delivery efficiency.[27−29] External stimulus including light, sound, magnetic field, and ionizing radiation can change the tumor microenvironment or

Received: July 13, 2021
Accepted: October 5, 2021

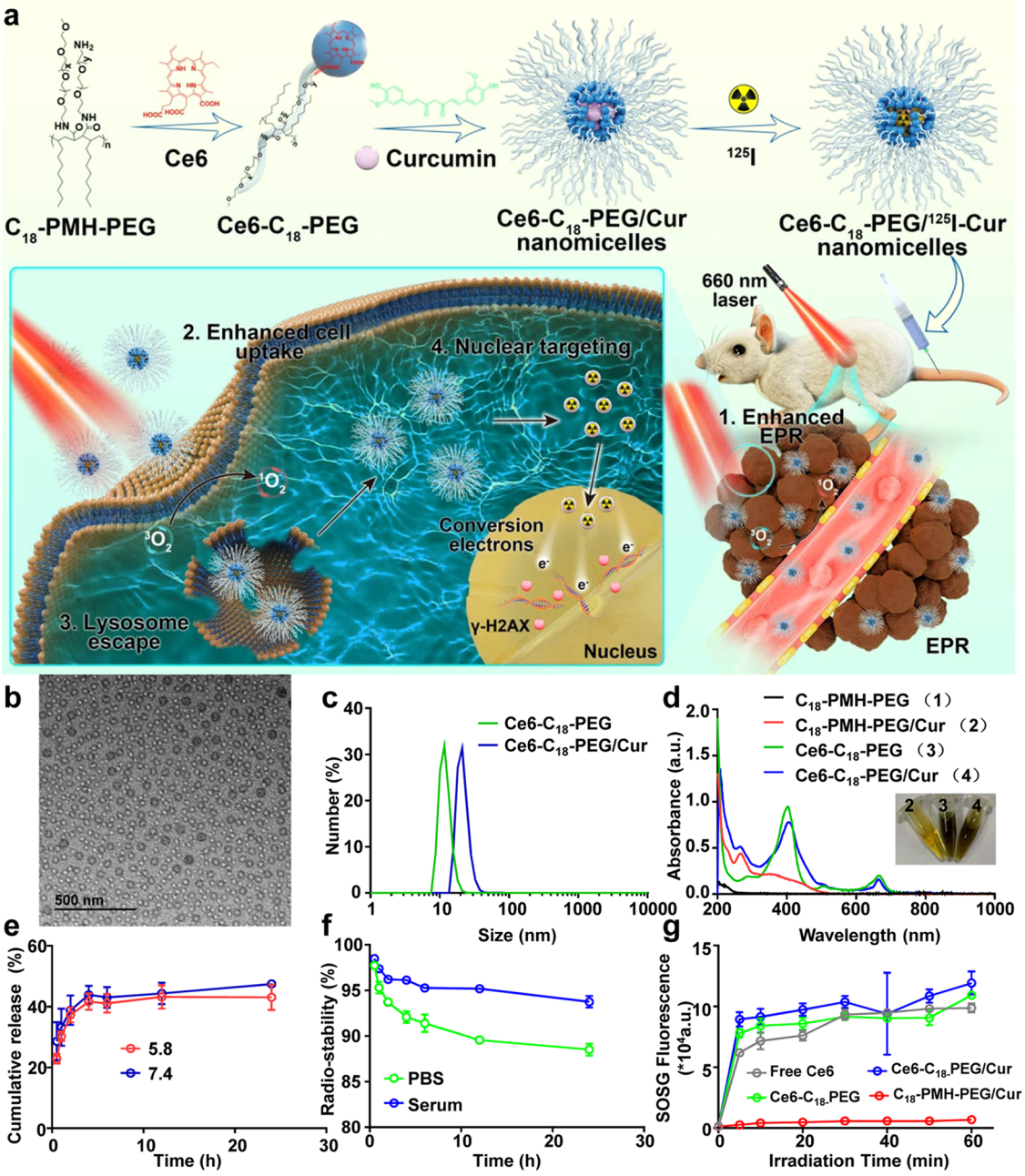

Figure 1. Preparation and characterization of Ce6-C_{18}-PEG/Cur nanomicelles. (a) Schematic illustration of optimized delivery of ^{125}I for cancer theranostics under 660 nm laser irradiation. (b) Transmission electron microscope (TEM) image of Ce6-C_{18}-PEG/Cur nanomicelles. (c) Dynamic light scattering (DLS) data of Ce6-C_{18}-PEG nanomicelles with or without Cur loading. (d) Ultraviolet−visible−near-infrared (UV−vis−NIR) spectra of C_{18}-PMH-PEG, C_{18}-PMH-PEG/Cur, Ce6-C_{18}-PEG, and Ce6-C_{18}-PEG/Cur. (e) Release of Cur from Ce6-C_{18}-PEG/Cur in buffer solutions at pH 5.8 and pH 7.4. (f) Radiolabeling stability of Ce6-C_{18}-PEG/^{125}I-Cur incubated in PBS or serum on day 1. (g) Generation of singlet oxygen by measuring the fluorescence intensity changes of SOSG from free Ce6, Ce6-C_{18}-PEG, Ce6-C_{18}-PEG/Cur, and C_{18}-PMH-PEG/Cur at the same concentration of Ce6 (1 μg/mL). (e−g) Data are presented as mean ± standard deviation, n = 3.

tumor cell condition, resulting in optimized drug-loaded nanoparticle delivery.[30−35] Among them, dynamic therapy with light stimulation, termed photodynamic therapy (PDT), has been clinically approved for cancer treatment.[36−38] PDT is reported to improve the enhanced permeability and retention (EPR) effect in tumors and promote nanoparticle uptake and endo-lysosome escape by the tumor cell, leading to the step-by-step delivery of drugs for synergistic photodynamic−chemotherapy.[39−41]

In this work, we developed amphiphilic poly(ethylene glycol) (PEG) (poly(maleic anhydride-*alt*-1-octadecene)-poly(ethylene glycol) (C_{18}-PMH-PEG)) covalently grafted with a photosensitizer and then loaded with ^{125}I-labeled nucleus-targeting small-molecule drugs for fluorescence and single-photon emission computed tomography (FL/SPECT) imaging-guided internal conversion electronic therapy of cancer under 660 nm laser irradiation. First, the amphiphilic PEG with a bare amino group (C_{18}-PMH-PEG-NH_2) was obtained following our previous study[42] and then conjugated with chlorin e6 (Ce6) to form Ce6-C_{18}-PEG, which could further self-assemble with curcumin (Cur) to yield Ce6-C_{18}-PEG/Cur nanomicelles. Curcumin, containing a phenolic hydroxyl group

https://doi.org/10.1021/acsami.1c13249
ACS Appl. Mater. Interfaces XXXX, XXX, XXX−XXX

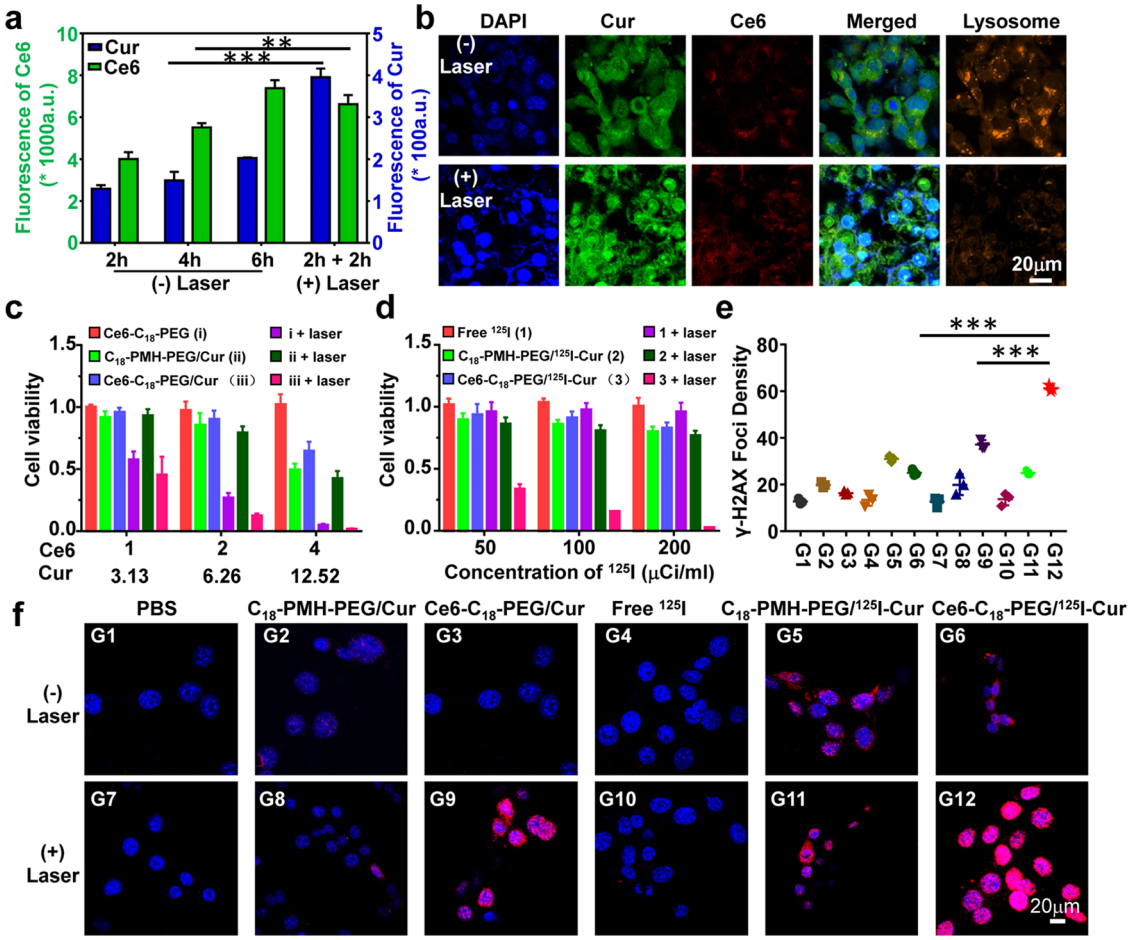

Figure 2. Optimized delivery of ^{125}I for nucleus-targeted internal conversion electron therapy of tumor cells under 660 nm laser irradiation. (a) Cellular uptake of Cur and Ce6 in 4T1 cells incubated with Ce6-C18-PEG/Cur at different times with or without laser exposure. (b) Confocal fluorescence images of 4T1 cells incubated with Ce6-C_{18}-PEG/Cur nanomicelles with or without 660 nm laser irradiation. (c) Relative viabilities of 4T1 cells treated by C_{18}-PMH-PEG/Cur, Ce6-C18-PEG, and Ce6-C_{18}-PEG/Cur with or without 660 nm laser irradiation. (d) Relative viabilities of 4T1 cells treated by free ^{125}I, C_{18}-PMH-PEG/^{125}I-Cur, and Ce6-C_{18}-PEG/^{125}I-Cur with or without 660 nm laser irradiation. (e) Quantitative analysis of γ-H2AX foci densities in each treatment group in Figure 2f. (f) Confocal fluorescence micrographs of γ-H2AX-stained 4T1 cells to visualize double-strand DNA breaks for cells treated with PBS, C_{18}-PMH-PEG/Cur, Ce6-C_{18}-PEG/Cur, free ^{125}I, C_{18}-PMH-PEG/^{125}I-Cur, and Ce6-C_{18}-PEG/^{125}I-Cur with or without 660 nm laser irradiation. Data are presented as mean ± standard deviation. Statistical analysis was performed using Student's two-tailed t-test (n = 3, *P < 0.05, **P < 0.01, ***P < 0.001).

for being labeled by radioactive iodine, was observed to enter the nucleus.[16] ^{125}I as a radioiodine can emit low-energy γ-rays and internal conversion electrons *via* orbital electron capture decay.[43−45] Two hours after intravenous (i.v.) injection with ^{125}I-labeled Ce6-C_{18}-PEG/Cur nanomicelles, the tumor could be accurately detected *via* the FL/SPECT imaging. Under the guidance of this bimodal imaging, a 660 nm laser was induced to irradiate the tumor tissue topically. The photodynamic reaction of Ce6 could enhance the EPR effect by destroying tumor blood vessels, increase the cellular uptake of ^{125}I-labeled Ce6-C_{18}-PEG/Cur, and promote lysosome escape of the nanoparticle. The released ^{125}I-labeled Cur was then transported into the nucleus, inducing the DNA double-strand break damage both *in vitro* and *in vivo*. Finally, this photo-driven combined treatment was proved to be safe for the treated animals (Figure 1a).

RESULTS AND DISCUSSION

In this study, photosensitizer-linked amphiphilic PEG (Ce6-C_{18}-PEG) was synthesized as described in the previously reported study.[22,23] ^{1}H-NMR confirmed the chemical structure of our prepared Ce6-C_{18}-PEG (Figure S1). This block polymer was then used to load the hydrophobic drug Cur. In brief, Cur was dissolved in sodium hydroxide (1 mL, 0.1 M) and mixed with Ce6-C_{18}-PEG. Then, the pH value of the solution was adjusted to 7.0 using hydrochloric acid (1 mL, 0.1 M) under the action of ultrasound. Cur disperses in alkaline water, while it precipitates in neutral water; thus, the Cur-loaded Ce6-C_{18}-PEG (Ce6-C_{18}-PEG/Cur) were obtained at pH 7.0 by centrifugation. The Ce6-C_{18}-PEG/Cur nanomicelles were first observed by transmission electron microscopy (TEM). The TEM images show that Ce6-C_{18}-PEG/Cur nanoparticles were spherical with a uniform size of about 20 nm (Figures 1b and S2). Dynamic light scattering (DLS) measured the hydrated ionic radius of the nanomicelles with or without Cur loading, showing that the Cur-loaded Ce6-C_{18}-PEG had a bigger size than naked Ce6-C_{18}-PEG, although both were between 10 and 30 nm (Figure 1c). Moreover, after incubating in different physiological solutions, including water, phosphate buffer saline (PBS), cell medium, and fetal bovine serum (FBS), for 1 day, the Ce6-C_{18}-PEG/Cur solution did not precipitate, and the nanomicelle sizes remained the same,

https://doi.org/10.1021/acsami.1c13249
ACS Appl. Mater. Interfaces XXXX, XXX, XXX−XXX

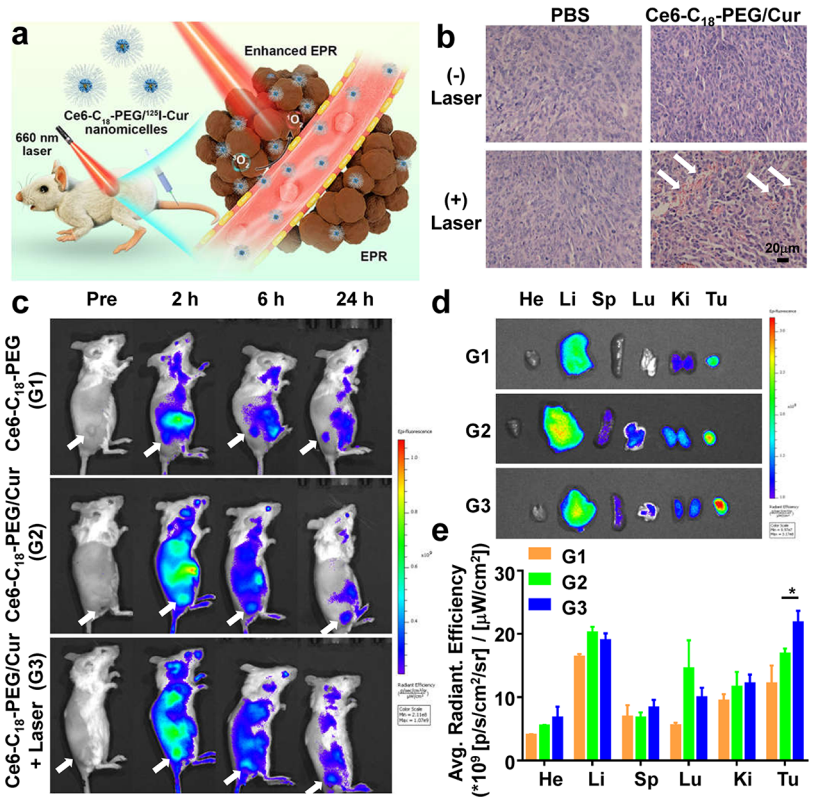

Figure 3. Enhanced EPR effect for Ce6-C_{18}-PEG/Cur nanomicelles under 660 nm laser irradiation. (a) Schematic illustration of a photodynamic reaction-enhanced EPR effect of a tumor. (b) H&E-stained tumor slices from mice with or without 660 nm laser irradiation; 660 nm laser irradiation was conducted at 2 h post injection of PBS or Ce6-C_{18}-PEG/Cur. (c) *In vivo* fluorescence images of 4T1 tumor-bearing mice treated with an i.v. injection of Ce6-C18-PEG, i.v. injection of Ce6-C18-PEG/Cur, or i.v. injection of Ce6-C_{18}-PEG/Cur plus 660 nm laser irradiation; 660 nm laser irradiation was conducted at 2 h post injection of Ce6-C_{18}-PEG/Cur. Tumors are indicated by white arrowheads. (d) *Ex vivo* fluorescence images of major organs and tumors dissected from mice in Figure 3c at 24 h p.i. (n = 3). (e) Biodistribution of Ce6 in 4T1 tumor-bearing mice in Figure 3 c at 24 h p.i. Data are presented as mean ± standard deviation. Statistical analysis was performed using Student's two-tailed t-test (n = 3, $^*P < 0.05$, $^{**}P < 0.01$, $^{***}P < 0.001$).

indicating the high biocompatibility of our as-prepared nanoparticles (Figure S3a,b). Hydrodynamic diameters and the ζ-potentials of Ce6-C_{18}-PEG/Cur in PBS solution were tested every other day for 1 week. The nanomicelles showed a stable size and surface ζ-potential, a prerequisite for its biomedicine applications (Figure S4).

Next, the ultraviolet−visible−near-infrared (UV−vis−NIR) absorbance spectra of Ce6-C_{18}-PEG and Ce6-C_{18}-PEG/Cur were analyzed to confirm the presence of the photosensitizer Ce6 and the nucleus-targeting drug Cur in Ce6-C_{18}-PEG/Cur particles. As shown in Figure 1d, Ce6-specific absorbance at 666 nm and the significant absorption of Cur at 265 nm appeared in the absorbance spectrum of Ce6-C_{18}-PEG/Cur. Afterward, the Ce6 concentration was measured by UV−visible spectrum, and the Cur concentration was tested by high-performance liquid chromatography. The results show that the loading rate and encapsulation efficiency of Cur in Ce6-C_{18}-PEG/Cur were 53.92 ± 1.71 and 21.5 ± 0.69%, respectively. Also, the mass rate of Ce6 to Cur in the nanoparticles was 1: (3.13 ± 0.15). The Ce6 and Cur release was then investigated in a PBS solution at pH 5.8 and 7.4. The covalent linkage between Ce6 and PEG prevented Ce6 release into the solution, while Cur was gradually released. More than 40% of Cur was released from Ce6-C_{18}-PEG/Cur at pH 5.8 and pH 7.4 (Figure 1e). Contrary to the drug release features of other drug delivery systems, Cur was released from Ce6-C_{18}-PEG/Cur at equal rates at pH 5.8 and 7.4, probably owing to the poor water solubility of Cur in an acidic solution.

Given the phenolic hydroxyl group of Cur, Ce6-C_{18}-PEG/Cur was labeled with ^{125}I. Using the iodogen-coating method, ^{125}I was labeled onto Ce6-C18-PEG or Ce6-C_{18}-PEG/Cur by a standard electrophilic substitution reaction. Radiolabeling yields of 2.23 ± 1.32% for naked Ce6-C18-PEG and 87.56 ± 4.43% for Ce6-C_{18}-PEG/Cur were obtained, suggesting that ^{125}I was labeled onto Cur. Furthermore, the radiostability of Ce6-C_{18}-PEG/^{125}I-Cur in PBS and mice serum was investigated by paper chromatography. After 24 h of incubation, 2 μL of Ce6-C_{18}-PEG/^{125}I-Cur or free ^{125}I was added in region 2, and 80% methanol was used as the developer. One hour later, the radioactivity of the added solutions and all regional papers was measured by a γ counter. Free ^{125}I was distributed mainly in regions 9 and 10. Regions 7 and 8 showed the yellow color of Cur and attributed to ^{125}I-Cur (Figure S5a,b). Thus, the detachment of ^{125}I from Ce6-C_{18}-PEG/^{125}I-Cur was measured, and the result indicated the limited deiodination from Ce6-C_{18}-PEG/^{125}I-Cur for 24 h, which was a prerequisite for subsequent biological applications (Figure 1f). Besides, these Ce6-contained nanomicelles could generate plenty of singlet oxygen under 660 nm laser irradiation (Figure 1g).

After acquiring this multifunctional nanomicelle, the cellular uptake and subcellular location of nanoparticles were explored under 660 nm laser exposure. Taking advantage of the inherent fluorescent properties of Ce6 and Cur, flow cytometry and

https://doi.org/10.1021/acsami.1c13249
ACS Appl. Mater. Interfaces XXXX, XXX, XXX−XXX

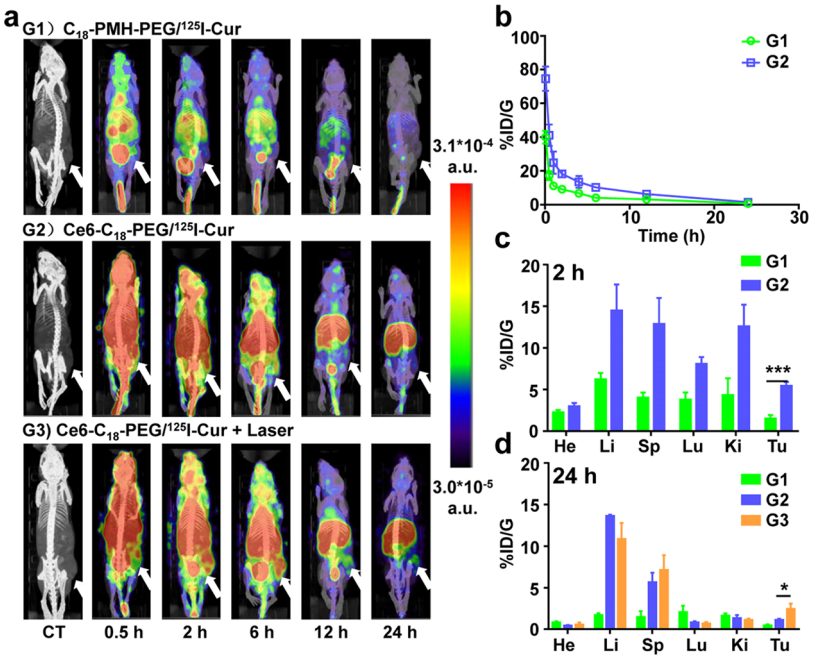

Figure 4. Enhanced EPR effect for Ce6-C_{18}-PEG/^{125}I-Cur nanomicelles under 660 nm laser irradiation. (a) Three-dimensional reconstructed SPECT/CT imaging of 4T1 tumor-bearing mice treated with an i.v. injection of C_{18}-PMH-PEG/^{125}I-Cur, i.v. injection of Ce6-C_{18}-PEG/^{125}I-Cur, or i.v. injection of Ce6-C_{18}-PEG/^{125}I-Cur plus 660 nm laser irradiation; 660 nm laser irradiation was conducted at 2 h post injection of Ce6-C_{18}-PEG/^{125}I-Cur. Tumors are indicated by the white arrowheads. (b) Blood circulation of C_{18}-PMH-PEG/^{125}I-Cur or Ce6-C_{18}-PEG/^{125}I-Cur after being i.v. injected into the mice. (c) Biodistribution of C_{18}-PMH-PEG/^{125}I-Cur and Ce6-C_{18}-PEG/^{125}I-Cur in the 4T1 tumor-bearing mice measured at 2 h post injection. (d) Biodistribution of ^{125}I in the 4T1 tumor-bearing mice treated with an i.v. injection of C_{18}-PMH-PEG/^{125}I-Cur, i.v. injection of Ce6-C_{18}-PEG/^{125}I-Cur, or i.v. injection of Ce6-C_{18}-PEG/^{125}I-Cur plus 660 nm laser irradiation; 660 nm laser irradiation was conducted at 2 h post injection of Ce6-C_{18}-PEG/^{125}I-Cur, and the biodistributions were measured at 24 h post injection. Data are presented as mean ± standard deviation. Statistical analysis was performed using Student's two-tailed *t*-test (n = 3, *P < 0.05, **P < 0.01, ***P < 0.001).

confocal microscopy were performed in cell experiments (Figure S6a,b). 4T1 murine breast cancer cells were incubated with Ce6-C_{18}-PEG/Cur, and 660 nm laser irradiation was conducted 2 h after incubation. As shown in Figure 2a, the cellular uptake of Ce6 and Cur gradually increased with time, which was further enhanced by 660 nm laser irradiation due to the increased cell membrane permeability caused by the generated singlet oxygen. Moreover, the nuclear entrance of Cur was observed under confocal microscopy, consistent with previously published work (Figure S7).[16] Upon 660 nm laser exposure, the lysosomes containing nanoparticles were destroyed, known as the PDT-triggered lysosome escape response.[35] Acridine orange (AO) is a pH-sensitive membrane-permeable fluorescent dye used to measure the integrity of the lysosomal membrane. When the lysosome membrane is intact, AO stays in the lysosome and fluoresces in red. However, when the lysosomal membrane is damaged, AO will deprotonate and emit green fluorescence. Figure S8 shows that 660 nm laser irradiation destroys the lysosome of 4T1 cells when incubated with Ce6-C_{18}-PEG/Cur. Afterward, the cells exposed to a 660 nm laser showed stronger Ce6 and Cur fluorescence intensity and more Cur released in their nucleus than nonirradiated cells (Figure 2b).

Considering that Ce6 is a photosensitizer and Cur is an antitumor herbal monomer in Chinese medicine, the photodynamic−chemotherapy properties of the Ce6-C_{18}-PEG/Cur nanomicelle against tumor cells were investigated. 4T1 cells were incubated with Ce6-C_{18}-PEG, C_{18}-PMH-PEG/Cur, or Ce6-C_{18}-PEG/Cur and irradiated by 660 nm laser (50 mW/cm^2, 10 min) after 2 h of incubation. The cell viability was measured 24 h after incubation. As shown in Figure 2c, only Ce6-containing nanomicelles exhibited strong phototoxicity and Cur-induced concentration-dependent cytotoxicity. A synergistic therapeutic effect was obtained using Ce6-C_{18}-PEG/Cur under 660 nm laser irradiation. Besides, based on the cellular uptake and subcellular location of Ce6-C_{18}-PEG/Cur, Ce6-C_{18}-PEG/^{125}I-Cur was expected to transport ^{125}I into the nucleus upon 660 nm laser exposure for internal conversion electronic therapy of cancer cells. C_{18}-PMH-PEG/Cur and Ce6-C_{18}-PEG/Cur nanoparticles promoted the cell delivery of ^{125}I, improving the cell-killing ability of ^{125}I at a limited level. Notably, combined with 660 nm laser irradiation, C_{18}-PMH-PEG/^{125}I-Cur was superior to C_{18}-PMH-PEG/Cur in the destruction of 4T1 cells, thus reflecting the effectiveness of ^{125}I therapy in cells (Figure 2d). Reactive oxygen species (ROS) production and DNA damage analysis revealed the therapeutic mechanism (Figures 2e,f and S9). Dihydroethidium (DHE) can enter living cells and be oxidized by intracellular ROS, forming ethyl oxide, which can be incorporated into chromosomal DNA to produce red fluorescence. As shown in Figure S9, Cur and the labeled ^{125}I induced limited ROS, and Ce6 only triggered abundant ROS under 660 nm laser irradiation. For DNA damage, free ^{125}I and PBS had no apparent damage to the cellular DNA. Cur-loaded nanoparticles could trigger limited DNA damage of cells with or without laser exposure, while ^{125}I labeling of the nanoparticles could increase the damage. Ce6-containing nanoparticles could induce significant DNA double-strand breaks under 660 nm laser irradiation. The most severe damage was observed in laser-irradiated Ce6-C_{18}-PEG/^{125}I-

https://doi.org/10.1021/acsami.1c13249
ACS Appl. Mater. Interfaces XXXX, XXX, XXX−XXX

Cur nanoparticles, consistent with the cell activity assay result shown in Figure 2c,d.

Encouraged by the excellent antitumor therapeutic efficacy of Ce6-C_{18}-PEG/^{125}I-Cur under laser irradiation *in vitro*, we then studied the nanomicelle capability for imaging-guided combined therapy of tumors *in vivo*. PDT could improve the EPR effect of tumor tissue *via* destroying the tumor vasculature (Figure 3a) consistent with a previous report.[36] Therefore, hematoxylin and eosin (H&E) staining of tumors collected from PBS- or Ce6-C_{18}-PEG/Cur-treated mice with or without 660 nm laser irradiation was performed. Significant angiolysis was observed only in the tumor slides of mice treated with Ce6-C_{18}-PEG/Cur plus laser exposure (Figure 3b). The fluorescence imaging system was used to detect the biodistribution of Ce6 in the 4T1 tumor-bearing mice treated with an i.v. injection of (G1) Ce6-C_{18}-PEG or (G2) Ce6-C_{18}-PEG/Cur and an i.v. injection of (G3) Ce6-C_{18}-PEG/Cur plus 660 nm laser irradiation at 2 h post injection (p.i.). Ce6-C_{18}-PEG or Ce6-C_{18}-PEG/Cur had abundant tumor accumulation at 2 h p.i. The Ce6 fluorescence intensity in tumor tissue was gradually decreased. Therefore, local irradiation of the tumor tissue with a 660 nm laser was conducted, resulting in prolonged retention of Ce6-C_{18}-PEG/Cur (Figure 3c). Twenty-four hours after the injection, the major organs, including the heart, liver, spleen, lung, and kidney, and the tumor tissues were collected and imaged by a fluorescence imaging system (Figure 3d). The tumor accumulation of Ce6-C_{18}-PEG/Cur was much higher than that of Ce6-C_{18}-PEG and could be further enhanced under 660 nm laser irradiation at 2 h p.i. (Figure 3d,e). Moreover, under a confocal microscope, Cur fluorescence was observed in the tumor tissues collected from the C_{18}-PMH-PEG/Cur or Ce6-C_{18}-PEG/Cur i.v. injected mice. As shown in Figure S10a,b, Ce6-C_{18}-PEG delivered more Cur into the tumor tissue than C_{18}-PMH-PEG. Meanwhile, 660 nm laser irradiation enhanced Cur accumulation in the tumors of mice injected with Ce6-C_{18}-PEG/Cur but not in those injected with C_{18}-PMH-PEG/Cur. Notably, the overlap between the nucleus and Cur increased after 660 nm laser irradiation in Ce6-C_{18}-PEG/Cur-injected mice, reflecting the PDT-enhanced nucleus targeting of Cur (Figure S10a). Thus, the light-driven delivery of Ce6-C_{18}-PEG/Cur was achieved.

After ^{125}I labeling, Ce6-C_{18}-PEG/Cur could deliver ^{125}I into the tumor tissue for SPECT imaging-guided antitumor therapy. First, considering the γ rays emitting ^{125}I, a SPECT imaging system was applied to image the nanoparticle-treated mice. As shown in Figure 4a, the radioactive signals were dispersed all over the body of C_{18}-PMH-PEG/^{125}I-Cur- and Ce6-C_{18}-PEG/^{125}I-Cur-injected mice at 30 min p.i. and located to the tumors at 2 h p.i., indicating the superior SPECT imaging efficacy of the particles. TEM and DLS were used to characterize the C_{18}-PMH-PEG/Cur particles. The result showed that C_{18}-PMH-PEG/Cur has no molded morphology and uncertain hydrated ionic radius with high polydisperse index (PDI), suggesting that C_{18}-PMH-PEG/Cur was not a stable nanoformulation but had high water solubility. In this form of Cur, C_{18}-PMH-PEG/^{125}I-Cur could be excreted in mice urine, supported by the strong SPECT signal of the bladder and the gradually decreasing signal in the whole body. In addition, Ce6-C_{18}-PEG/^{125}I-Cur exhibited better SPECT imaging efficacy of tumor at 2 h p.i., which could be used for tumor tissue localization and guide the follow-up treatment. Moreover, the strong SPECT signal in the tumor could be maintained longer by 660 nm laser irradiation at 2 h p.i. of Ce6-C_{18}-PEG/^{125}I-Cur, reflecting that PDT optimized the tumor accumulation of this radioactive nanoparticle.

Next, the blood circulation profiles of C_{18}-PMH-PEG/^{125}I-Cur and Ce6-C_{18}-PEG/^{125}I-Cur were quantitatively detected using a γ counter to measure the radioactivity in blood samples. The blood circulation followed a classical two-compartment model with first and second phase blood circulation half-lives of 0.13 ± 0.018 and 4.78 ± 0.89 h for C_{18}-PMH-PEG/^{125}I-Cur and 0.24 ± 0.11 and 6.08 ± 0.43 h for Ce6-C_{18}-PEG/^{125}I-Cur. Moreover, the ^{125}I biodistribution in mice treated with C_{18}-PMH-PEG/^{125}I-Cur and Ce6-C_{18}-PEG/^{125}I-Cur was measured at 2 and 24 h p.i. A high tumor accumulation and tolerable accumulation in normal organs, including the heart, liver, spleen, lung, and kidney, were observed at 2 h p.i. The ^{125}I accumulation ratios between tumor and normal organs were calculated. Compared with the abdominal viscera such as the liver, spleen, and kidney, organs in the chest, including the heart and lung, retained less ^{125}I-Cur (Figure S11a). Therefore, SPECT/FL imaging-guided 660 nm laser irradiation based on Ce6-C_{18}-PEG/^{125}I-Cur would best treat the tumors far away from the abdomen, such as breast cancer, to limit local PDT side effects. At 24 h p.i., almost 79.33 ± 2.51% of Ce6-C_{18}-PEG/^{125}I-Cur radioactivity in the tumor was diminished owing to decreased body circulation of the nanoparticle plus the release of ^{125}I-Cur from the nanoparticle (Figure 4c,d). However, only 54.93 ± 11.82% of Ce6-C_{18}-PEG/^{125}I-Cur radioactivity in the tumor was cleared when the tumors were irradiated by a 660 nm laser, further indicating the PDT-optimized ^{125}I delivery *in vivo* (Figures 4d and S11b).

Motivated by high tumor accumulation and optimized nucleus-targeted delivery of Ce6-C_{18}-PEG/^{125}I-Cur under 660 nm laser irradiation, the *in vivo* antitumor therapy was carried out on 4T1 tumor-bearing mice. The mice were randomly divided into eight groups (five mice per group). The different treatments were as follows: Group 1: i.v. injection with PBS; Group 2: i.v. injection with C_{18}-PMH-PEG/Cur; Group 3: i.v. injection with Ce6-C_{18}-PEG/Cur; Group 4: i.v. injection with free ^{125}I; Group 5: i.v. injection with Ce6-C_{18}-PEG/^{125}I-Cur; Group 6: i.v. injection with PBS plus 660 nm laser irradiation (50 mW/cm^2, 10 min); Group 7: i.v. injection with Ce6-C_{18}-PEG/Cur plus 660 nm laser irradiation; and Group 8: i.v. injection with Ce6-C_{18}-PEG/^{125}I-Cur plus 660 nm laser irradiation. The laser irradiation was carried out at 2 h p.i. Tumor volume and mice body weights were recorded every 2 days. First, Ce6-C_{18}-PEG was a better carrier of Cur than C_{18}-PMH-PEG to induce tumor growth inhibition. Second, injection of free ^{125}I almost had no therapeutic effect, while Ce6-C_{18}-PEG/^{125}I-Cur showed more significant antitumor efficacy than Ce6-C_{18}-PEG/Cur, reflecting the successful nucleus-targeted delivery of ^{125}I p.i. of Ce6-C_{18}-PEG/^{125}I-Cur. Moreover, 660 nm laser irradiation of tumor further enhanced the antitumor effect of Ce6-C_{18}-PEG/Cur and Ce6-C_{18}-PEG/^{125}I-Cur. The performance enhancement of Ce6-C_{18}-PEG/^{125}I-Cur was much higher than that of Ce6-C_{18}-PEG/Cur, owing to the strong DNA damage efficiency of the endonuclear ^{125}I (Figure 5a). According to the tumor growth curves, mice survival curves were recorded when the tumor volume was greater than 1000 mm^3. The result showed the prolonged survival time of the mice i.v. injected with Ce6-C_{18}-PEG/^{125}I-Cur plus 660 nm laser irradiation (Group 8) (Figure S12). In addition, the mice in each group showed no physical

https://doi.org/10.1021/acsami.1c13249
ACS Appl. Mater. Interfaces XXXX, XXX, XXX−XXX

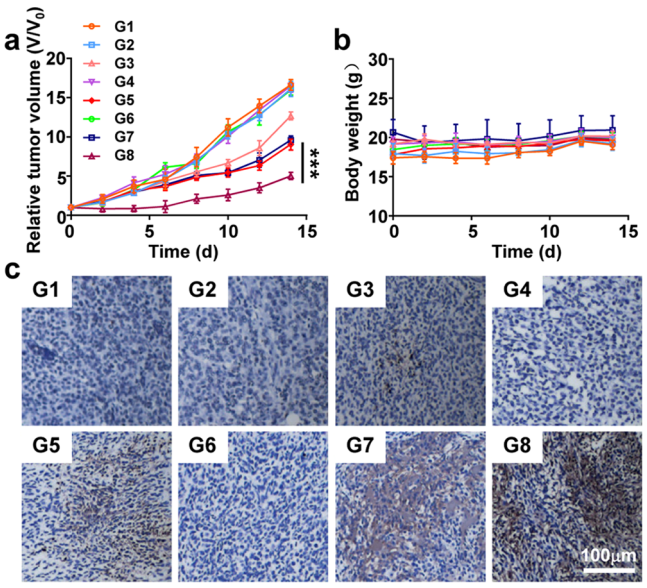

Figure 5. *In vivo* antitumor therapy. (a) Tumor growth curves of mice undergoing different treatments. Five mice were used for each group. Error bars are based on standard errors of the mean (SEM). The different treatments were as follows: G1: i.v. injection with PBS; G2: i.v. injection with C_{18}-PMH-PEG/Cur; G3: i.v. injection with Ce6-C_{18}-PEG/Cur; G4: i.v. injection with free ^{125}I; G5: i.v. injection with Ce6-C_{18}-PEG/^{125}I-Cur; G6: i.v. injection with PBS plus 660 nm laser irradiation (50 mW/cm^2, 10 min); G7: i.v. injection with Ce6-C_{18}-PEG/Cur plus 660 nm laser irradiation; and G8: i.v. injection with Ce6-C_{18}-PEG/^{125}I-Cur plus 660 nm laser irradiation. (b) Average body weight of mice after various treatments indicated. Five mice were used in each group. Error bars are based on standard deviation (SD). (c) Representative terminal deoxynucleotidyl transferase dUTP nick-end labeling (TUNEL) staining images of tumor slices collected from different groups of mice. Data are presented as mean ±standard error of means. Statistical analysis was performed using Student's two-tailed *t*-test ($n = 5$, $^*P < 0.05$, $^{**}P < 0.01$, $^{***}P < 0.001$).

changes initially, indicating a high degree of safety of the treatment (Figure 5b). Therefore, Ce6-C_{18}-PEG/^{125}I-Cur nanomicelles could be used as a carrier of Cur and ^{125}I for optimized therapy of tumors under 660 nm laser exposure.

Next, to study the therapeutic mechanism of various treatments, ROS production and apoptosis analysis by DHE staining, hematoxylin and eosin (H&E) staining, and terminal deoxynucleotidyl transferase dUTP nick-end labeling (TUNEL) assay were performed to the treated tumor cells (Figures S13, S14, and 5c). The tumors collected from control groups, including groups 1, 4, and 6, showed almost limited ROS production. Ce6-C_{18}-PEG as a Cur carrier induced more ROS than C_{18}-PMH-PEG, and ^{125}I labeling further increased ROS production. Moreover, 660 nm laser irradiation triggered more pronounced ROS production for Ce6-containing nanoparticles, especially Ce6-C_{18}-PEG/^{125}I-Cur. Also, apoptosis could be induced in tumor sections collected from mice with different treatments according to ROS production. At 30 days post treatment, the major organs, including the heart, liver, spleen, lung, and kidney in groups 1 and 8, were collected for H&E staining. The mice treated with Ce6-C_{18}-PEG/^{125}I-Cur plus laser irradiation showed no noticeable inflammation or damage (Figure S15). Therefore, we believe our strategy will enable effective photodynamic-chemo-internal conversion electron therapy for cancer treatment with a high safety profile.

Finally, we should pay close attention to the biosafety of drug-loaded nanomedicines owing to the prolonged blood circulation time and changed biodistribution of their loading drugs. First, the biodistribution of Ce6-C_{18}-PEG/^{125}I-Cur nanoparticles was measured at 1, 3, 5, and 7 days post i.v. injection of the nanomicelles. Although ^{125}I-Cur accumulation in the liver/spleen was relatively high at 1 day p.i., the ^{125}I-Cur accumulation in these organs could gradually decrease in 1 week, and ^{125}I-Cur accumulation in the major organs was below 1.5% ID/G after 7 days of injection (Figure 6a). To explore the elimination pathways of the loaded ^{125}I-Cur, urine and feces were collected from the mice injected with Ce6-C_{18}-PEG/^{125}I-Cur. As shown in Figure 6b, most of the ^{125}I-Cur was excreted *via* urine and feces. Furthermore, the blood samples were collected from the healthy and treated mice for blood analysis and histological examinations. The liver/kidney function markers and blood cell classification measurements of Ce6-C_{18}-PEG/^{125}I-Cur to the treated mice were within the normal range, indicating no significant side effects of Ce6-C_{18}-PEG/^{125}I-Cur to the treated mice (Figure 6c). Besides, Ce6-C_{18}-PEG/^{125}I-Cur-treated mice showed no apparent morphologic change of cells or inflammatory exudation in their major organs, including the heart, liver, spleen, lung, and kidney (Figure 6d). Thus, the i.v. injection of Ce6-C_{18}-PEG/^{125}I-Cur was with high biosafety. More importantly, in our antitumor strategy, 660 nm laser irradiation was performed in local tumor sites under the guidance of SPECT/FL imaging, and the tumor type in our study was breast cancer, which is far from the liver and spleen. Therefore, our antitumor strategy was safe for the 4T1 tumor-bearing mice.

CONCLUSIONS

In summary, Ce6-C_{18}-PEG was prepared to self-assemble with Cur, obtaining Ce6-C_{18}-PEG/Cur nanomicelles as an efficient carrier of ^{125}I for biomedical applications. ^{125}I can emit γ rays, which could be used for isotopic tracing and SPECT imaging and several internal conversion electrons, killing tumor cells when used as high LET radiation. First, SPECT/FL imaging was applied to image the tumor-bearing mice injected with Ce6-C_{18}-PEG/^{125}I-Cur, providing the precise localization of tumor tissue to guide the follow-up local therapy. Afterward, taking advantage of the nucleus-targeting properties of Cur, the nanoparticle transported ^{125}I into the nucleus *in vitro* and *in vivo*, leading to the DNA damage of tumor cells. More importantly, plenty of singlet oxygen generated from Ce6 optimized the delivery of Ce6-C_{18}-PEG/^{125}I-Cur at various stages, including tumor accumulation, cellular uptake, and lysosome escape under 660 nm laser irradiation, resulting in a more significant therapeutic effect of internal conversion electrons. Finally, this photo-driven combined therapy was proved to be safe for the treated mice. Therefore, our work develops a novel strategy to deliver ^{125}I into the nucleus efficiently under the local laser irradiation for the ideal antitumor treatment with high safety.

EXPERIMENTAL METHODS

Materials. Poly(maleic anhydride-*alt*-1-octadecene) (C_{18}-PMH) and BOC-PEG-NH_2 were purchased from Guangzhou Carbide Technology Co., Ltd. Triethylamine was purchased from Sinopharm Chemical Reagent Co., Ltd. 1-(3-Dimethylaminopropyl)-3-ethylcarbodiimine hydrochloride (EDC) was purchased from Sigma-Aldrich. Methoxy-poly(ethylene glycol)-amino (mPEG-NH_2, 5K) was purchased from Shanghai Pengshuo Biological Technology Co., Ltd.

https://doi.org/10.1021/acsami.1c13249
ACS Appl. Mater. Interfaces XXXX, XXX, XXX−XXX

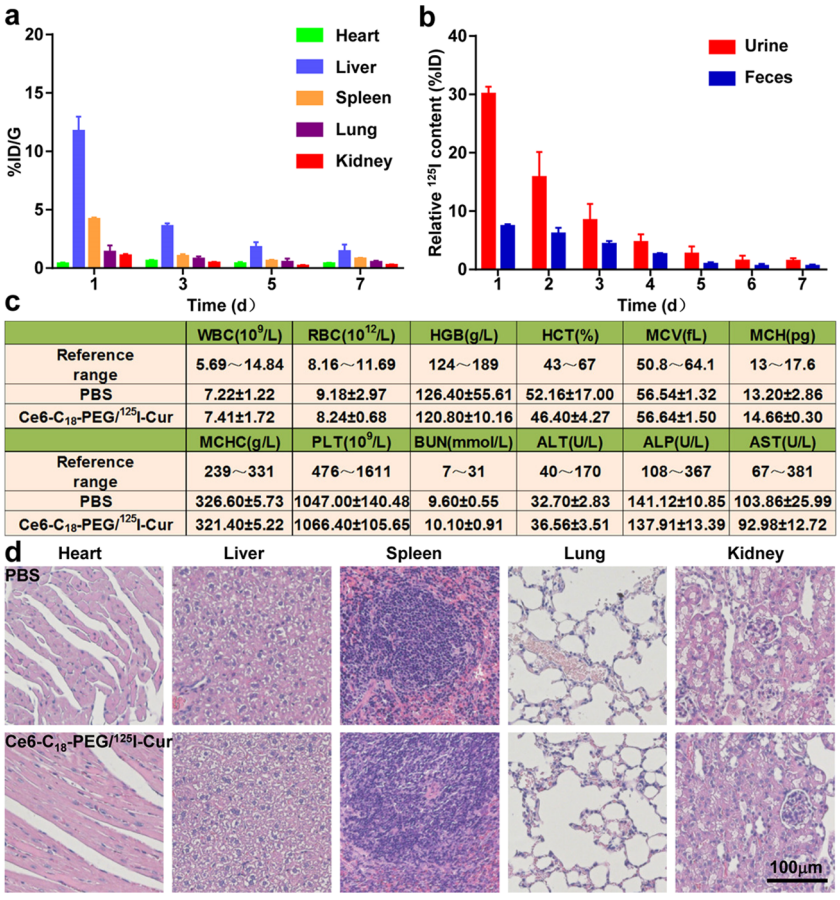

	WBC(10^9/L)	RBC(10^{12}/L)	HGB(g/L)	HCT(%)	MCV(fL)	MCH(pg)
Reference range	5.69∼14.84	8.16∼11.69	124∼189	43∼67	50.8∼64.1	13∼17.6
PBS	7.22±1.22	9.18±2.97	126.40±55.61	52.16±17.00	56.54±1.32	13.20±2.86
Ce6-C_{18}-PEG/^{125}I-Cur	7.41±1.72	8.24±0.68	120.80±10.16	46.40±4.27	56.64±1.50	14.66±0.30
	MCHC(g/L)	PLT(10^9/L)	BUN(mmol/L)	ALT(U/L)	ALP(U/L)	AST(U/L)
Reference range	239∼331	476∼1611	7∼31	40∼170	108∼367	67∼381
PBS	326.60±5.73	1047.00±140.48	9.60±0.55	32.70±2.83	141.12±10.85	103.86±25.99
Ce6-C_{18}-PEG/^{125}I-Cur	321.40±5.22	1066.40±105.65	10.10±0.91	36.56±3.51	137.91±13.39	92.98±12.72

Figure 6. Biosafety of Ce6-C_{18}-PEG/^{125}I-Cur. (a) Biodistribution of Ce6-C_{18}-PEG/^{125}I-Cur measured at 1, 3, 5, and 7 days post injection (n = 3). (b) Content of ^{125}I in feces and urine at different time points post i.v. injection of Ce6-C_{18}-PEG/^{125}I-Cur (n = 3). (c) Blood biochemistry and hematological data (including white blood cells (WBCs), red blood cells (RBCs), hemoglobin (HGB), hematocrit (HCT), mean corpuscular volume (MCV), mean corpuscular hemoglobin (MCH), mean corpuscular hemoglobin concentration (MCHC), platelets (PLT), blood urea nitrogen (BUN), alanine aminotransferase (ALT), alkaline phosphatase (ALP), and aspartate aminotransferase (AST) levels) of healthy female Balb/c mice treated with PBS or Ce6-C_{18}-PEG/^{125}I-Cur at day 7 post injection (5 mice/group). (d) Representative H&E-stained images of major organs, including the liver, spleen, kidney, lung, and heart collected from the untreated mice and Ce6-C_{18}-PEG/^{125}I-Cur-treated mice at day 7 post injection. The doses of Ce6, Cur, and ^{125}I were 5 mg/kg, 15.65 mg/kg, and 500 μCi per mouse, respectively. No obvious organ damage or lesion was observed for Ce6-C_{18}-PEG/^{125}I-Cur-treated mice. Data are presented as mean ± standard deviation.

Trifluoroacetic acid (TFA) and chlorin e6 were purchased from Shanghai McLean Co., Ltd. Curcumin was purchased from Aladdin. Sodium hydroxide, hydrochloric acid, dichloromethane, and dimethyl sulfoxide (DMSO) were purchased from Shanghai Lingfeng Chemical Reagent Co., Ltd. ^{125}I was purchased from Shanghai Xinke Pharmaceutical Co., Ltd.

Preparation of Ce6-C_{18}-PEG. First, we synthesized NH_2-C_{18}PMH-PEG as described in our previously published work.[42] Briefly, 10 mg of C_{18}-PMH and 96 mg of BOC-PEG-NH_2 were dissolved with 3 mL of dichloromethane. Under stirring, 6 μL of triethylamine and 6 mg of EDC were added to the solution. After 12 h, 143 mg of mPEG-NH_2 (5K) and 6 mg EDC were added and stirred for another 24 h. The solution was blow-dried with nitrogen, and 4 mL of TFA was added and stirred for 4 h. TFA was dried with nitrogen, and the product was dissolved in water and dialyzed in deionized water for 2 days. The NH_2-C_{18}-PMH-PEG powder was obtained after lyophilization of the final solution.

Then, we prepared Ce6-C18-PEG *via* the covalent binding of NH_2-C_{18}-PMH-PEG and Ce6. Seventeen milligrams of Ce6, 15 mg of EDC, and 15 mg of *N*-hydroxythioimine succinate were dissolved in 4 mL of DMSO and stirred for 1 h. Fifty milligrams of NH_2-C_{18}-PMH-PEG dissolved in 4 mL of DMSO was added into the above solution. After 24 h, the solution was dialyzed in deionized water for 2 days, followed by lyophilization to obtain Ce6-C_{18}-PEG.

Preparation of Ce6-C_{18}-PEG/Cur. Twenty milligrams of curcumin (Cur) powder was dissolved in 1 mL of 0.1 M NaOH and added into 5 mL of deionized water. Then, 50 mg of Ce6-C_{18}-PEG was added and stirred in the dark for 2 h. Under stirring, 1 mL of 0.1 M HCl was added into the solution dropwise. Then, the solution was sonicated for 1.5 h and stirred overnight. The solution was centrifuged at 14 800 rpm for 10 min three times to collect the supernatant and remove the precipitated free Cur. Finally, Ce6-C_{18}-PEG/Cur was further refined and concentrated with an ultrafiltration tube (10 kD). The Ce6 and Cur concentrations in Ce6-C_{18}-PEG/Cur solutions were measured using UV−vis spectrometric determination and high-performance liquid chromatography.

^{125}I Labeling. The iodogen-coating method was selected to label ^{125}I onto the nanomicelles as described in our previous work.[46] Briefly, 0.2 mL of Ce6-C_{18}-PEG/Cur (5 mg/mL of Ce6) and 5 mCi of Na^{125}I were added into an iodogen-coated EP tube and vortexed for 30 min at room temperature. ^{125}I-labeled Ce6-C18-PEG/Cur was purified by removing the unbonded radioiodine by ultrafiltration (10 kD). To test the Ce6-C18-PEG/^{125}I-Cur radiostability, the nanoparticle was incubated in PBS and mice serum at 37°C. Paper chromatography was used to isolate the free ^{125}I at the appointed incubation time when 80% methanol was used as the developing solvent. A γ counter was used to measure the percent of peeled ^{125}I (n = 3).

https://doi.org/10.1021/acsami.1c13249
ACS Appl. Mater. Interfaces XXXX, XXX, XXX−XXX

Cellular Uptake and Cellular Sublocalization of Ce6-C_{18}-PEG/Cur. Flow cytometer and laser scanning confocal microscope were used to detect the cellular uptake and cellular sublocalization of Ce6-C_{18}-PEG/Cur, respectively. 4T1 cells preseeded into six-well plates at a density of 2×10^5 per well were incubated with Ce6-C_{18}-PEG/Cur (1 μg/mL of Ce6 and 3.13 μg/mL of Cur). At the appointed time, the cells were collected and washed with PBS three times. The Ce6 and Cur fluorescence intensity of every cell was measured by flow cytometry (n = 3). 4T1 cells were planted into the 24-well plates with round slides in the bottom at the density of 5×10^4 per well. After incubating with Ce6-C_{18}-PEG/Cur and irradiating by 660 nm laser, the 4T1 cells were stained by 4′,6-diamidino-2-phenylindole (DAPI) and washed three times. A confocal microscope was applied to observe the distribution of Ce6 and Cur in the cell.

Cytotoxicity Experiment. To test the Ce6-C_{18}-PEG/Cur cytotoxicity with or without 660 nm laser irradiation, 4T1 cells preseeded into 96-well plates were incubated with different concentrations of nanomicelles. Laser exposure (50 mW/cm^2, 10 min) with 660 nm was conducted at 2 h incubation time. The standard methyl thiazolyltetrazolium assay determined the relative cell viabilities at 24 h incubation time (n = 3).

Immunofluorescence Analysis of γ-H2AX. The γ-H2AX expression in DNA is often used to reflect the extent of DNA damage. 4T1 cells were seeded in 24-well plates with round slides in the bottom and incubated with cell medium containing PBS, C_{18}-PMH-PEG/Cur, Ce6-C_{18}-PEG/Cur, free ^{125}I, C_{18}-PMH-PEG/^{125}I-Cur or Ce6-C_{18}-PEG/^{125}I-Cur for 2 h and then irradiated by 660 nm laser at a power of 50 mW/cm^2. After irradiation, the cells were incubated for another 2 h and fixed in 4% paraformaldehyde for 10 min. γ-H2AX and nuclear stains were performed according to a reported protocol.[47] Then, the cells were observed by confocal microscopy (n = 3).

FL/SPECT Imaging. Female BALB/c mice were purchased from Nanjing Pengsheng Biological Technology Co., Ltd., and used under protocols approved by the Animal Ethics Committee of Nantong University. 4T1 tumor-bearing mice were generated after 4T1 cells were planted onto the right side of the back of mice. When the volume of the tumors reached about 60−100 mm^3, the tumor-bearing mice were selected for further experiments. Mice were i.v. injected with Ce6-C_{18}-PEG or Ce6-C_{18}-PEG/Cur (5 mg/kg of Ce6) and imaged by a small animal fluorescence imaging system. Similarly, mice i.v. injected with C_{18}-PMH-PEG/^{125}I-Cur or Ce6-C_{18}-PEG/^{125}I-Cur (500 μCi of ^{125}I per mouse) were imaged by *in vivo* animal SPECT (MILabs, Utrecht, the Netherlands) imaging system at appointed time points. The 660 nm laser irradiation was induced at 2 h p.i. of the nanoparticles.

Blood Circulation and Biodistribution. Healthy female Balb/C mice were i.v. injected with C_{18}-PMH-PEG/^{125}I-Cur or Ce6-C_{18}-PEG/^{125}I-Cur (20 μCi of ^{125}I per mouse). At various time points p.i., the radioactivity of the collected blood samples from the orbital vein in mice was measured by a γ counter (n = 3). Also, the major healthy organs and tumors were collected, weighed, and their radioactivity was measured (n = 3). The 660 nm laser irradiation was induced at 2 h p.i. of Ce6-C_{18}-PEG/^{125}I-Cur.

Antitumor Therapy *In Vivo*. 4T1 tumor-bearing mice were randomly divided into eight groups (five mice in each group) and subjected to different treatments. The treatments were (i) i.v. injection with PBS, (ii) i.v. injection with C_{18}-PMH-PEG/Cur, (iii) i.v. injection with Ce6-C_{18}-PEG/Cur, (iv) i.v. injection with free ^{125}I, (v) i.v. injection with Ce6-C_{18}-PEG/^{125}I-Cur, (vi) i.v. injection with PBS plus 660 nm laser irradiation (50 mW/cm^2, 10 min), (vii) i.v. injection with Ce6-C_{18}-PEG/Cur plus 660 nm laser irradiation, (viii) i.v. injection with Ce6-C_{18}-PEG/^{125}I-Cur plus 660 nm laser irradiation. The doses of Ce6, Cur, and ^{125}I in all groups were 5 mg/kg, 15.65 mg/kg, and 500 μCi per mouse, respectively. Laser exposure was carried out at 2 h p.i. The tumor sizes and body weights were monitored every 2 days. On day 3, tumors were collected from each group and used for H&E and TUNEL staining. The H&E staining of major organs, including the heart, liver, spleen, lung, and kidney collected from groups i and viii at day 30, was also performed to check the potential toxicity of our strategy to the treated mice.

■ ASSOCIATED CONTENT

Supporting Information

The Supporting Information is available free of charge at https://pubs.acs.org/doi/10.1021/acsami.1c13249.

^{1}H-NMR spectra of Ce6-C_{18}-PEG, TEM image, and DLS measurements of Ce6-C_{18}-PEG/Cur, radioactive paper chromatography of Ce6-C_{18}-PEG/^{125}I-Cur, nucleus targeting and ROS production experiments, and H&E staining images (PDF)

■ AUTHOR INFORMATION

Corresponding Author

Xuan Yi − *School of Pharmacy, Jiangsu Key Laboratory of Inflammation and Molecular Drug Targets, Nantong University, Nantong, Jiangsu 226001, China;* orcid.org/0000-0002-5287-6608; Email: xuanyi@ntu.edu.cn

Authors

Yuanyuan Qin − *School of Pharmacy, Jiangsu Key Laboratory of Inflammation and Molecular Drug Targets, Nantong University, Nantong, Jiangsu 226001, China; Department of Pharmacy, Suzhou Hospital of Traditional Chinese Medicine, Suzhou, Jiangsu 215009, China*

Mengling Shen − *School of Pharmacy, Jiangsu Key Laboratory of Inflammation and Molecular Drug Targets, Nantong University, Nantong, Jiangsu 226001, China*

Xinpei Liu − *School of Pharmacy, Jiangsu Key Laboratory of Inflammation and Molecular Drug Targets, Nantong University, Nantong, Jiangsu 226001, China*

Jingyu Gu − *School of Pharmacy, Jiangsu Key Laboratory of Inflammation and Molecular Drug Targets, Nantong University, Nantong, Jiangsu 226001, China*

Minqian Zhu − *School of Pharmacy, Jiangsu Key Laboratory of Inflammation and Molecular Drug Targets, Nantong University, Nantong, Jiangsu 226001, China*

Complete contact information is available at: https://pubs.acs.org/10.1021/acsami.1c13249

Author Contributions

§Y.Q. and M.S. contributed equally to this paper.

Notes

The authors declare no competing financial interest.

■ ACKNOWLEDGMENTS

This work was partially supported by the National Natural Science Foundation of China (31900986, U2032134), Young Medical Talents of Jiangsu Province (QNRC20162612), Gusu Health Talents Training Project (GSWS2020083), and Suzhou Science and Technology Development Project (SYS2019106).

■ REFERENCES

(1) Zhu, D.; Liu, Z.; Li, Y.; Huang, Q.; Xia, L.; Li, K. Delivery of Manganese Carbonyl to the Tumor Microenvironment Using Tumor-Derived Exosomes for Cancer Gas Therapy and Low Dose Radiotherapy. *Biomaterials* **2021**, *274*, No. 120894.

(2) Zhang, C.; Yan, L.; Wang, X.; Dong, X.; Zhou, R.; Gu, Z.; Zhao, Y. Tumor Microenvironment-Responsive Cu2(OH)PO4 Nanocrystals for Selective and Controllable Radiosentization via the X-ray-Triggered Fenton-like Reaction. *Nano Lett.* **2019**, *19*, 1749−1757.

(3) Takeshima, T.; Pop, L. M.; Laine, A.; Iyengar, P.; Vitetta, E. S.; Hannan, R. Key Role for Neutrophils in Radiation-Induced Antitumor Immune Responses: Potentiation with G-CSF. *Proc. Natl. Acad. Sci. U.S.A* **2016**, *113*, 11300−11305.
(4) White, J. M.; Escorcia, F. E.; Viola, N. T. Perspectives on Metals-Based Radioimmunotherapy (RIT): Moving Forward. *Theranostics* **2021**, *11*, 6293−6314.
(5) Durante, M.; Orecchia, R.; Loeffler, J. S. Charged-Particle Therapy in Cancer: Clinical Uses and Future Perspectives. *Nat. Rev. Clin. Oncol.* **2017**, *14*, 483−495.
(6) Tommelein, J.; De Vlieghere, E.; Verset, L.; Melsens, E.; Leenders, J.; Descamps, B.; Debucquoy, A.; Vanhove, C.; Pauwels, P.; Gespach, C. P.; Vral, A.; De Boeck, A.; Haustermans, K.; de Tullio, P.; Ceelen, W.; Demetter, P.; Boterberg, T.; Bracke, M.; De Wever, O. Radiotherapy-Activated Cancer-Associated Fibroblasts Promote Tumor Progression through Paracrine IGF1R Activation. *Cancer Res.* **2018**, *78*, 659−670.
(7) Tsujii, H.; Mizoe, J.; Kamada, T.; Baba, M.; Kato, S.; Kato, H.; Tsuji, H.; Yamada, S.; Yasuda, S.; Ohno, T.; Yanagi, T.; Hasegawa, A.; Sugawara, T.; Ezawa, H.; Kandatsu, S.; Yoshikawa, K.; Kishimoto, R.; Miyamoto, T. Overview of Clinical Experiences on Carbon Ion Radiotherapy at MRS. *Radiother. Oncol.* **2004**, *73*, S41−S49.
(8) Chiblak, S.; Tang, Z.; Lemke, D.; Knoll, M.; Dokic, I.; Warta, R.; Moustafa, M.; Meir, W.; Brons, S.; Rapp, C.; Muschal, S.; Seidel, P.; Bendzsus, M.; Adeberg, S.; Wiestler, O. D.; Haberkorn, U.; Debus, J.; Herold-Mende, C.; Wick, W.; Abdollahi, A. Carbon Irradiation Overcomes Glioma Radioresistance by Eradicating Stem Cells and Forming an Antiangiogenic and Immunopermissive Niche. *JCI Insight* **2019**, *4*, No. e123837.
(9) Aghevlian, S.; Boyle, A. J.; Reilly, R. M. Radioimmunotherapy of Cancer with High Linear Energy Transfer (LET) Radiation Delivered by Radionuclides Emitting Alpha-Particles or Auger Electrons. *Adv. Drug Delivery Rev.* **2017**, *109*, 102−118.
(10) Dekempeneer, Y.; Caveliers, V.; Ooms, M.; Maertens, D.; Gysemans, M.; Lahoutte, T.; Xavier, C.; Lecocq, Q.; Maes, K.; Covens, P.; Miller, B. W.; Bruchertseifer, F.; Morgenstern, A.; Cardinaels, T.; D'Huyvetter, M. Therapeutic Efficacy of (213)Bi-Labeled sdAbs in a Preclinical Model of Ovarian Cancer. *Mol. Pharm.* **2020**, *17*, 3553−3566.
(11) Miederer, M.; McDevitt, M. R.; Sgouros, G.; Kramer, K.; Cheung, N. K. V.; Scheinberg, D. A. Pharmacokinetics, Dosimetry, and Toxicity of the Targetable Atomic Generator, Ac-225-HuM195, in Nonhuman Primates. *J. Nucl. Med.* **2004**, *45*, 129−137.
(12) Yan, C. Y.; Shi, W. G.; Gu, J. W.; Lee, R. J.; Zhang, Y. Design of a Novel Nucleus-Targeted NLS-KALA-SA Nanocarrier to Delivery Poorly Water-Soluble Anti-Tumor Drug for Lung Cancer Treatment. *J. Pharm. Sci.* **2021**, *110*, 2432−2441.
(13) Yang, Y.; Zhu, W.; Feng, L.; Chao, Y.; Yi, X.; Dong, Z.; Yang, K.; Tan, W.; Liu, Z.; Chen, M. G-Quadruplex-Based Nanoscale Coordination Polymers to Modulate Tumor Hypoxia and Achieve Nuclear-Targeted Drug Delivery for Enhanced Photodynamic Therapy. *Nano Lett.* **2018**, *18*, 6867−6875.
(14) Zhang, X.; Zhu, T.; Miao, Y.; Zhou, L.; Zhang, W. Dual-Responsive Doxorubicin-Loaded Nanomicelles for Enhanced Cancer Therapy. *J. Nanobiotechnol.* **2020**, *18*, No. 136.
(15) Zhang, Z.; Xu, W.; Xiao, P.; Kang, M.; Yan, D.; Wen, H.; Song, N.; Wang, D.; Tang, B. Z. Molecular Engineering of High-Performance Aggregation-Induced Emission Photosensitizers to Boost Cancer Theranostics Mediated by Acid-Triggered Nucleus-Targeted Nanovectors. *ACS Nano* **2021**, *15*, 10689−10699.
(16) Zheng, P.; Ding, B.; Shi, R.; Jiang, Z.; Xu, W.; Li, G.; Ding, J.; Chen, X. A Multichannel Ca(2+) Nanomodulator for Multilevel Mitochondrial Destruction-Mediated Cancer Therapy. *Adv. Mater.* **2021**, *33*, No. 2007426.
(17) Zhang, P.; Huang, H.; Banerjee, S.; Clarkson, G. J.; Ge, C.; Imberti, C.; Sadler, P. J. Nucleus-Targeted Organoiridium-Albumin Conjugate for Photodynamic Cancer Therapy. *Angew. Chem., Int. Ed.* **2019**, *58*, 2350−2354.
(18) Chen, M.; Yang, D.; Sun, Y.; Liu, T.; Wang, W.; Fu, J.; Wang, Q.; Bai, X.; Quan, G.; Pan, X.; Wu, C. In Situ Self-Assembly Nanomicelle Microneedles for Enhanced Photoimmunotherapy via Autophagy Regulation Strategy. *ACS Nano* **2021**, *15*, 3387−3401.
(19) Li, C.; Zhou, J.; Wu, Y.; Dong, Y.; Du, L.; Yang, T.; Wang, Y.; Guo, S.; Zhang, M.; Hussain, A.; Xiao, H.; Weng, Y.; Huang, Y.; Wang, X.; Liang, Z.; Cao, H.; Zhao, Y.; Liang, X. J.; Dong, A.; Huang, Y. Core Role of Hydrophobic Core of Polymeric Nanomicelle in Endosomal Escape of siRNA. *Nano Lett.* **2021**, *21*, 3680−3689.
(20) Li, M.; Li, S.; Zhou, H.; Tang, X.; Wu, Y.; Jiang, W.; Tian, Z.; Zhou, X.; Yang, X.; Wang, Y. Chemotaxis-Driven Delivery of Nano-Pathogenoids for Complete Eradication of Tumors Post-Phototherapy. *Nat. Commun.* **2020**, *11*, No. 1126.
(21) Cheng, L.; Jiang, D.; Kamkaew, A.; Valdovinos, H. F.; Im, H. J.; Feng, L.; England, C. G.; Goel, S.; Barnhart, T. E.; Liu, Z.; Cai, W. Renal-Clearable PEGylated Porphyrin Nanoparticles for Image-guided Photodynamic Cancer Therapy. *Adv. Funct. Mater.* **2017**, *27*, No. 1702928.
(22) Cheng, L.; Kamkaew, A.; Sun, H.; Jiang, D.; Valdovinos, H. F.; Gong, H.; England, C. G.; Goel, S.; Barnhart, T. E.; Cai, W. Dual-Modality Positron Emission Tomography/Optical Image-Guided Photodynamic Cancer Therapy with Chlorin e6-Containing Nanomicelles. *ACS Nano* **2016**, *10*, 7721−7730.
(23) Gong, H.; Dong, Z.; Liu, Y.; Yin, S.; Cheng, L.; Xi, W.; Xiang, J.; Liu, K.; Li, Y.; Liu, Z. Engineering of Multifunctional Nano-Micelles for Combined Photothermal and Photodynamic Therapy Under the Guidance of Multimodal Imaging. *Adv. Funct. Mater.* **2014**, *24*, 6492−6502.
(24) Han, K.; Lei, Q.; Jia, H.-Z.; Wang, S.-B.; Yin, W.-N.; Chen, W.-H.; Cheng, S.-X.; Zhang, X.-Z. A Tumor Targeted Chimeric Peptide for Synergistic Endosomal Escape and Therapy by Dual-Stage Light Manipulation. *Adv. Funct. Mater.* **2015**, *25*, 1248−1257.
(25) Han, K.; Lei, Q.; Wang, S.-B.; Hu, J.-J.; Qiu, W.-X.; Zhu, J.-Y.; Yin, W.-N.; Luo, X.; Zhang, X.-Z. Dual-Stage-Light-Guided Tumor Inhibition by Mitochondria-Targeted Photodynamic Therapy. *Adv. Funct. Mater* **2015**, *25*, 2961−2971.
(26) Cheng, Y. J.; Hu, J. J.; Qin, S. Y.; Zhang, A. Q.; Zhang, X. Z. Recent Advances in Functional Mesoporous Silica-Based Nanoplatforms for Combinational Photo-Chemotherapy of Cancer. *Biomaterials* **2020**, *232*, No. 119738.
(27) Zhen, S.; Yi, X.; Zhao, Z.; Lou, X.; Xia, F.; Tang, B. Z. Drug Delivery Micelles with Efficient Near-Infrared Photosensitizer for Combined Image-Guided Photodynamic Therapy and Chemotherapy of Drug-Resistant Cancer. *Biomaterials* **2019**, *218*, No. 119330.
(28) Dhaliwal, A.; Zheng, G. Improving Accessibility of EPR-Insensitive Tumor Phenotypes Using EPR-Adaptive Strategies: Designing a New Perspective in Nanomedicine Delivery. *Theranostics* **2019**, *9*, 8091−8108.
(29) Yu, B.; Wei, H.; He, Q.; Ferreira, C. A.; Kutyreff, C. J.; Ni, D.; Rosenkrans, Z. T.; Cheng, L.; Yu, F.; Engle, J. W.; Lan, X.; Cai, W. Efficient Uptake of (177) Lu-Porphyrin-PEG Nanocomplexes by Tumor Mitochondria for Multimodal-Imaging-Guided Combination Therapy. *Angew. Chem., Int. Ed.* **2018**, *57*, 218−222.
(30) Han, X.; Chen, J.; Chu, J.; Liang, C.; Ma, Q.; Fan, Q.; Liu, Z.; Wang, C. Platelets as Platforms for Inhibition of Tumor Recurrence Post-Physical Therapy by Delivery of Anti-PD-L1 Checkpoint Antibody. *J. Controlled Release* **2019**, *304*, 233−241.
(31) Liang, C.; Chao, Y.; Yi, X.; Xu, J.; Feng, L.; Zhao, Q.; Yang, K.; Liu, Z. Nanoparticle-Mediated Internal Radioisotope Therapy to Locally Increase the Tumor Vasculature Permeability for Synergistically Improved Cancer Therapies. *Biomaterials* **2019**, *197*, 368−379.
(32) Passarella, R. J.; Spratt, D. E.; van der Ende, A. E.; Phillips, J. G.; Wu, H.; Sathiyakumar, V.; Zhou, L.; Hallahan, D. E.; Harth, E.; Diaz, R. Targeted Nanoparticles that Deliver a Sustained, Specific Release of Paclitaxel to Irradiated Tumors. *Cancer Res.* **2010**, *70*, 4550−4559.
(33) Song, X.; Zhang, R.; Liang, C.; Chen, Q.; Gong, H.; Liu, Z. Nano-Assemblies of J-Aggregates Based on a NIR Dye as a

https://doi.org/10.1021/acsami.1c13249
ACS Appl. Mater. Interfaces XXXX, XXX, XXX−XXX

Multifunctional Drug Carrier for Combination Cancer Therapy. *Biomaterials* **2015**, *57*, 84−92.
(34) Tian, B.; Wang, C.; Zhang, S.; Feng, L.; Liu, Z. Photothermally Enhanced Photodynamic Therapy Delivered by Nano-Graphene Oxide. *ACS Nano* **2011**, *5*, 7000−7009.
(35) Zhang, H.; Wang, T.; Qiu, W.; Han, Y.; Sun, Q.; Zeng, J.; Yan, F.; Zheng, H.; Li, Z.; Gao, M. Monitoring the Opening and Recovery of the Blood-Brain Barrier with Noninvasive Molecular Imaging by Biodegradable Ultrasmall Cu2- xSe Nanoparticles. *Nano Lett.* **2018**, *18*, 4985−4992.
(36) Tian, J.; Xu, L.; Xue, Y.; Jiang, X.; Zhang, W. Enhancing Photochemical Internalization of DOX through a Porphyrin-based Amphiphilic Block Copolymer. *Biomacromolecules* **2017**, *18*, 3992−4001.
(37) Wang, Y.; Wei, G.; Zhang, X.; Xu, F.; Xiong, X.; Zhou, S. A Step-by-Step Multiple Stimuli-Responsive Nanoplatform for Enhancing Combined Chemo-Photodynamic Therapy. *Adv. Mater.* **2017**, *29*, No. 1605357.
(38) Zhen, Z.; Tang, W.; Chuang, Y.-J.; Todd, T.; Zhang, W.; Lin, X.; Niu, G.; Liu, G.; Wang, L.; Pan, Z.; Chen, X.; Xie, J. Tumor Vasculature Targeted Photodynamic Therapy for Enhanced Delivery of Nanoparticles. *ACS Nano* **2014**, *8*, 6004−6013.
(39) Zeng, Z.; Zhang, C.; Li, J.; Cui, D.; Jiang, Y.; Pu, K. Activatable Polymer Nanoenzymes for Photodynamic Immunometabolic Cancer Therapy. *Adv. Mater.* **2021**, *33*, No. e2007247.
(40) Cui, D.; Huang, J.; Zhen, X.; Li, J.; Jiang, Y.; Pu, K. A Semiconducting Polymer Nano-prodrug for Hypoxia-Activated Photodynamic Cancer Therapy. *Angew. Chem., Int. Ed.* **2019**, *58*, 5920−5924.
(41) Yang, G. G.; Hao, L.; Cao, Q.; Zhang, H.; Yang, J.; Ji, L. N.; Mao, Z. W. Three-in-One Self-Assembled Nanocarrier for Dual-Drug Delivery, Two-Photon Imaging, and Chemo-Photodynamic Synergistic Therapy. *ACS Appl. Mater. Interfaces* **2018**, *10*, 28301−28313.
(42) Yi, X.; Yang, K.; Liang, C.; Zhong, X. Y.; Ning, P.; Song, G. S.; Wang, D. L.; Ge, C. C.; Chen, C. Y.; Chai, Z. F.; Liu, Z. Imaging-Guided Combined Photothermal and Radiotherapy to Treat Subcutaneous and Metastatic Tumors Using Iodine-131-Doped Copper Sulfide Nanoparticles. *Adv. Funct. Mater.* **2015**, *25*, 4689−4699.
(43) Cao, J.; Wei, Y.; Zhang, Y.; Wang, G.; Ji, X.; Zhong, Z. Iodine-Rich Polymersomes Enable Versatile SPECT/CT Imaging and Potent Radioisotope Therapy for Tumor in Vivo. *ACS Appl. Mater. Interfaces* **2019**, *11*, 18953−18959.
(44) Yang, Y.; Xie, Q.; Zhao, Z.; He, L.; Chan, L.; Liu, Y.; Chen, Y.; Bai, M.; Pan, T.; Qu, Y.; Ling, L.; Chen, T. Functionalized Selenium Nanosystem as Radiation Sensitizer of (125)I Seeds for Precise Cancer Therapy. *ACS Appl. Mater. Interfaces* **2017**, *9*, 25857−25869.
(45) Imstepf, S.; Pierroz, V.; Raposinho, P.; Bauwens, M.; Felber, M.; Fox, T.; Shapiro, A. B.; Freudenberg, R.; Fernandes, C.; Gama, S.; Gasser, G.; Motthagy, F.; Santos, I. R.; Alberto, R. Nuclear Targeting with an Auger Electron Emitter Potentiates the Action of a Widely Used Antineoplastic Drug. *Bioconjugate Chem.* **2015**, *26*, 2397−2407.
(46) Yi, X.; Xu, M. Y.; Zhou, H. L.; Xiong, S. S.; Qian, R.; Chai, Z. F.; Zhao, L.; Yang, K. Ultrasmall Hyperbranched Semiconducting Polymer Nanoparticles with Different Radioisotopes Labeling for Cancer Theranostics. *ACS Nano* **2018**, *12*, 9142−9151.
(47) Zhu, D.; Lyu, M.; Huang, Q.; Suo, M.; Liu, Y.; Jiang, W.; Duo, Y.; Fan, K. Stellate Plasmonic Exosomes for Penetrative Targeting Tumor NIR-II Thermo-Radiotherapy. *ACS Appl. Mater. Interfaces* **2020**, *12*, 36928−36937.

https://doi.org/10.1021/acsami.1c13249
ACS Appl. Mater. Interfaces XXXX, XXX, XXX−XXX